ARTICLE

An atomically precise Pt_{17} nanocluster: their electronic structure and high activity for a hydrogen evolution reaction

Kazutaka Oiwa[a,†], Kaoru Ikeda[a,†], Ryuki Kurosaki[a], Kotaro Sato[a], Naoki Nishi[a], Haruna Tachibana[a], Md. Ahsanul Haque[a], Tokuhisa Kawawaki[a,c,*], Kenji Iida[b,*], and Yuichi Negishi[a,c,d,*]
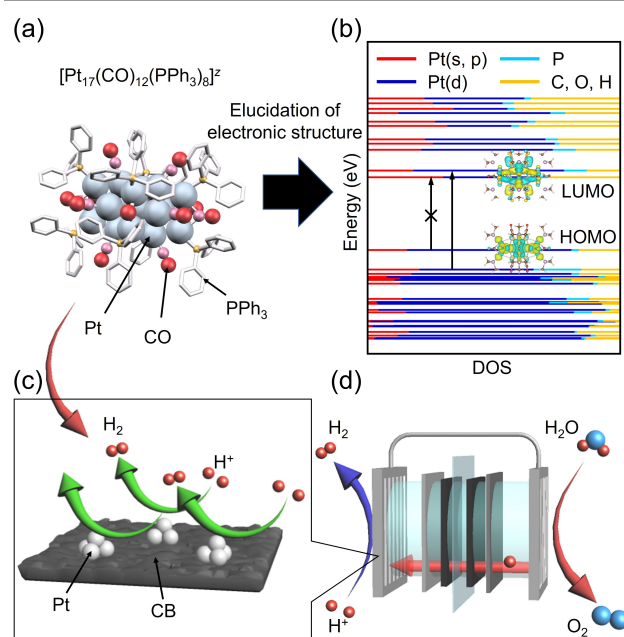
Pt nanoclusters (Pt NCs) approximately 1 nm in size show potential as catalysts owing to their large specific surface areas and unique electronic structures, which are influenced by quantum size effects. However, synthesizing Pt NCs with atomic precision under ambient conditions remains challenging, with $[Pt_{17}(CO)_{12}(PPh_3)_8]^z$ (z = 1+ or 2+; CO = carbon monoxide; PPh_3 = triphenylphosphine) being the only current example of such a NC. It exhibits extraordinary stability, and its electronic structure and catalytic utility in a range of reactions are topics of widespread interest. In this study, we reveal its electronic structure and explore its catalytic activity in the hydrogen evolution reaction (HER). Our findings revealed that $[Pt_{17}(CO)_{12}(PPh_3)_8]^z$ possesses a discrete electronic structure, with the HOMO and LUMO primarily constituted by the s, p, and d orbitals of Pt; that a Pt_{17} NC-supported carbon-black catalyst (Pt_{17}/CB) achieves 3.59-times the HER mass activity of a commercially available Pt/CB catalyst; and that the optimal electronic structure of the surface Pt atoms in Pt_{17}/CB significantly enhances its HER activity. These insights underscore the potential of leveraging atomically precise Pt NCs in the design and development of highly active electrocatalysts for water splitting.

Introduction

The synthesis of ~1-nm-sized Pt nanoclusters (Pt NCs) and their alloy NCs has garnered significant interest owing to their unique properties and potential applications in catalysis. Using carbon monoxide (CO) ligands,[1,2] Pt NCs ($Pt_n(CO)_m$ NCs; where n and m are the numbers of Pt atoms and CO ligands, respectively) can be synthesized with atomic precision.[3-6] Most such NCs are not stable under atmospheric conditions, and thus few studies have been conducted on their application. However, a recently developed method for the synthesis of Pt NCs under atmospheric conditions using CO and phosphines (PR_3) or thiolates (SR) as ligands ($Pt_n(CO)_m(PR_3)_l$ or $Pt_n(CO)_m(SR)_o$ NCs, respectively) has emerged as a simple and convenient way to generate such NCs in large quantities.[7-12]

In particular, $[Pt_{17}(CO)_{12}(PPh_3)_8]^z$ (z = 1+ or 2+; PPh_3 = triphenylphosphine; Fig. 1a) represents a unique form of Pt NCs that can be synthesized under atmospheric conditions and exhibit remarkable stability. These NCs not only are structurally distinct but also serve as highly effective precursors of catalysts for reactions, including CO oxidation, propylene oxidation, and oxygen reduction.[8,11,13] Their robust catalytic activity highlights their potential, making them invaluable in the development of high-performance catalysts for various fields. However, the

a. Department of Applied Chemistry, Faculty of Science, Tokyo University of Science, 1-3 Kagurazaka, Shinjuku-ku, Tokyo 162-8601, Japan. E-mail: kawawaki@rs.tus.ac.jp
b. Institute for Catalysis, Hokkaido University, Sapporo, Hokkaido 001–0021, Japan. E-mail: k-iida@cat.hokudai.ac.jp
c. Research Institute for Science and Technology, Tokyo University of Science, 2641 Yamazaki, Noda, Chiba, Japan.
d. Institute of Multidisciplinary Research for Advanced Materials, Tohoku University, Katahira 2-1-1, Aoba-ku, Sendai 980-8577, Japan. E-mail: yuichi.negishi.a8@tohoku.ac.jp

† These authors contributed equally to this work.
* Corresponding author

Fig. 1 Schematic of the work performed in this study. (a) Geometric and (b) calculated electronic structure of $[Pt_{17}(CO)_{12}(PPh_3)_8]^z$ and their catalytic application to the (c) HER for (d) water electrolysis.

origins of the unique electronic properties of $[Pt_{17}(CO)_{12}(PPh_3)_8]^z$ remain unclear.

Density functional theory (DFT) calculations may provide valuable insights into the underlying reasons for the high stability and catalytic activity of $[Pt_{17}(CO)_{12}(PPh_3)_8]^z$. Such study could also help predict the geometric and electronic structures of other potentially stable $Pt_n(CO)_m(PR_3)_l$ NCs that could be synthesized in the future.[14-19]

With ongoing depletion of fossil resources and global warming, the transition to a hydrogen (H_2)-based energy economy is increasingly necessary. Currently, H_2 is predominantly produced from methane derived from natural gas and coal, which are fossil fuels. Thus, to reduce its environmental impact, water electrolysis using electricity supplied by renewable energy sources has gained significant attention as a method for H_2 production (Fig. S1).[20,21] Water electrolysis involves both the hydrogen evolution reaction (HER) and the oxygen evolution reaction (OER), where H_2 is generated through the reduction of water in the HER. Among the various water electrolysis systems, proton exchange membrane water electrolyzers (PEMWEs) are particularly attractive owing to their compact size, high energy efficiency, high H_2-production rate, and quick response to voltage fluctuations. However, the widespread adoption of PEMWEs faces a major challenge: the need of stable and active electrocatalysts that can operate effectively under acidic conditions.

Currently, Pt metals, which are precious and expensive, are the only materials that meet these requirements.[22,23] Consequently, reducing the amount of Pt used in PEMWE electrocatalysts is critical for making this technology more economically viable and environmentally sustainable. Using $[Pt_{17}(CO)_{12}(PPh_3)_8]^z$ (Fig. 1a) as a precursor to deposit Pt_{17} NCs on carbon black (CB; Pt_{17}/CB) is a promising strategy to enhance the activity of HER catalysts while decreasing overall Pt usage. Using ~1 nm-Pt NCs increases the number of active sites for the reaction, potentially leading to catalysts that are more efficient than typical CB catalysts loaded with larger (~2−3 nm) Pt nanoparticles (Pt NPs) commonly used in PEMWEs. Additionally, DFT calculations can provide insight into the electronic structure, high stability, and catalytic activity of these small Pt NCs, guiding the future design of highly active and stable electrocatalysts for the HER.[13]

Accordingly, in the present study, we aimed to elucidate the electronic structure of $[Pt_{17}(CO)_{12}(PPh_3)_8]^z$ using DFT calculations (Fig. 1b); develop an HER catalyst with enhanced activity compared with commercial Pt NPs/CB by using $[Pt_{17}(CO)_{12}(PPh_3)_8]^z$ as a precursor (Fig. 1c); and determine the origin of the high HER activity exhibited by Pt_{17}/CB (Fig. 1d). Our results revealed that the transition from the highest occupied molecular orbital (HOMO) to the lowest unoccupied molecular orbital (LUMO) in $[Pt_{17}(CO)_{12}(PPh_3)_8]^{2+}$ is forbidden and that the orbitals neighbouring them primarily comprise the s, p, and d orbitals of Pt. Additionally, we successfully created a Pt_{17}/CB catalyst with an HER mass activity 3.59-times that of commercially available Pt NPs/CB. The DFT calculations also strongly suggested that the high HER activity of Pt_{17}/CB arises from the presence of Pt atoms with an optimal electronic structure for the HER.

Results and discussion

Elucidation of the electronic structure of atomically precise $[Pt_{17}(CO)_{12}(PPh_3)_8]^z$

$[Pt_{17}(CO)_{12}(PPh_3)_8]^z$ was synthesized through a polyol reduction and ligand-exchange method,[24-29] similar to that in previous reports.[11,13,30] Briefly, the Pt precursor was heated to 120 °C in ethylene glycol with sodium hydroxide under atmospheric conditions. The solution was then cooled to room temperature, and PPh₃ was added to form $Pt_n(CO)_m(PPh_3)_l$ NCs. From the obtained products, $[Pt_{17}(CO)_{12}(PPh_3)_8]^z$ was selectively isolated using solvent extraction. The resulting product was confirmed to be high-purity $[Pt_{17}(CO)_{12}(PPh_3)_8]^z$ via electrospray ionization mass spectrometry (ESI-MS; Fig. S2). Figure 2a shows the optical absorption spectrum of $[Pt_{17}(CO)_{12}(PPh_3)_8]^z$, which presents prominent peaks at approximately 1.10, 1.20, 1.85, and 2.15 eV, indicating a discrete electronic structure similar to that of $Au_{25}(PET)_{18}$ (PET = 2-phenylethanethiolate) and its alloy NCs.[31-34]

DFT calculations were conducted to elucidate the origin of peaks observed in the optical absorption spectrum of $[Pt_{17}(CO)_{12}(PPh_3)_8]^z$ by the Gaussian 16 program,[35] and B3LYP functional[36-38] was adopted (basis set; the Stuttgard/Dresden basis set with effective core potentials[39] for Pt, 6-311+G* for P, C, O, and H). This study focused on the closed-shell electronic systems of $[Pt_{17}(CO)_{12}(PPh_3)_8]^{2+}$ owing to the computational complexity of the open-shell systems in $[Pt_{17}(CO)_{12}(PPh_3)_8]^{1+}$. To reduce computational burden, the phenyl groups (Ph₃) were replaced with methyl groups $(CH_3)_3$.[40] Geometry optimization was performed based on the structure of $[Pt_{17}(CO)_{12}(PPh_3)_8]^{2+}$ obtained by single crystal X-ray diffraction (Fig. 3a), followed by time-dependent (TD)-DFT calculations for the optical absorption spectrum using the optimized geometric structure of $[Pt_{17}(CO)_{12}(PPh_3)_8]^{2+}$.
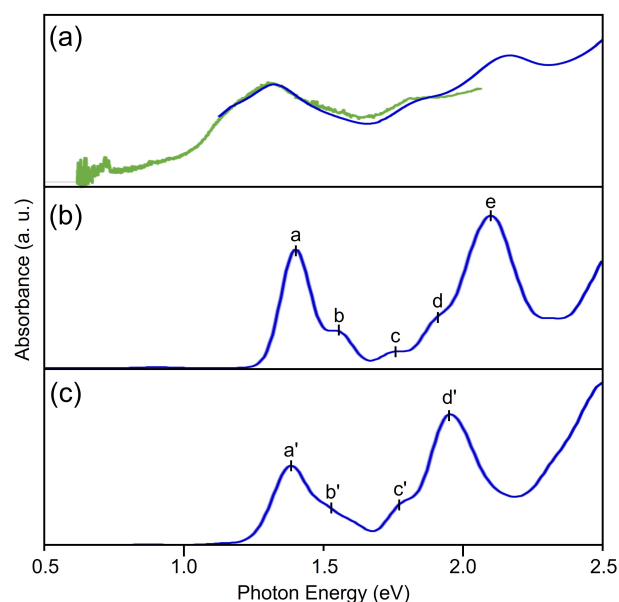
**Fig. 2** Optical absorbance spectrum of (a) $[Pt_{17}(CO)_{12}(PPh_3)_8]^z$ (z = 1+, 2+) and the calculated absorption spectra of (b) $Pt_{17}(CO)_{12}(P(CH_3)_3)_8]^{2+}$ and (c) $[Pt_{17}(CO)_{12}(PPh_3)_8]^{2+}$.

ARTICLE

The optimized structure $[Pt_{17}(CO)_{12}(P(CH_3)_3)_8]^{2+}$ (Fig. 3b) features an icosahedral Pt_{13} core surrounded by CO, μ_2–CO, $P(CH_3)_3$, and capping $Pt_2(\mu_2$–CO$)_2(P(CH_3)_3)_2$ ligands. This structure closely matches that obtained experimentally for $[Pt_{17}(CO)_{12}(PPh_3)_8]^{2+}$ (Fig. 3a and Fig. S3).[11] The calculated spectrum of $[Pt_{17}(CO)_{12}(P(CH_3)_3)_8]^{2+}$ (Fig. 2b) shows peaks at approximately 1.40, 1.55, 1.75, and 2.10 eV, which correspond well with the experimental spectrum of $[Pt_{17}(CO)_{12}(PPh_3)_8]^z$ (Fig. 2a).

We also conducted calculations using the Los Alamos (LANL2DZ) basis set with effective core potentials[41,42] to examine how the choice of basis set affects the spectral shape. The results revealed that both the geometric structure (Fig. S4) and optical absorption spectrum (Fig. S5) remain largely consistent with those obtained using other basis functions. To explore the impact on the spectral characteristics of substituting Ph_3 with CH_3, we performed calculations for $[Pt_{17}(CO)_{12}(PPh_3)_8]^{2+}$ using the LANL2DZ basis function, and obtained a geometric structure (Fig. 3c) and optical absorption spectrum (Fig. 2c) similar to those of $[Pt_{17}(CO)_{12}(P(CH_3)_3)_8]^{2+}$. The overall similarity in both the geometric structure and the spectral shape indicates that 1) the calculated optical absorption spectra are relatively insensitive to the choice of

basis set and functional group substitution, and 2) the calculated results are in good agreement with experimental observations.

Figure 4A shows the density of states (DOSs) for the orbitals ranging from HOMO−20 to LUMO+10, calculated for $[Pt_{17}(CO)_{12}(P(CH_3)_3)_8]^{2+}$ (basis set; SDD for Pt, 6-311 + G* for P, C, O, and H). It was revealed that the orbitals near the HOMO and LUMO primarily comprise the s, p, and d orbitals of Pt (Fig. 4AB). Owing to the high symmetry of $[Pt_{17}(CO)_{12}(P(CH_3)_3)_8]^{2+}$, the transition from HOMO to LUMO is forbidden (Fig. 3b), and thus it is not observed (at 0.74 eV) in the experimental optical absorption spectrum (Fig. 2a). The peak around 1.40 eV is attributed to transitions from HOMO−1,2,3,4 to LUMO or LUMO+1, whereas the peak near 1.55 eV is due to transitions from HOMO−5 to LUMO+1. The peak around 2.10 eV involves multiple transitions, including those from orbitals below HOMO−10 to LUMO, as well as transitions from orbitals near HOMO to LUMO+1 and the orbitals above. Further analysis using the LANL2DZ basis set confirmed that the DOSs of $[Pt_{17}(CO)_{12}(PPh_3)_8]^{2+}$ are not significantly influenced by the choice of basis set nor functional group substitutions (Fig. S6).
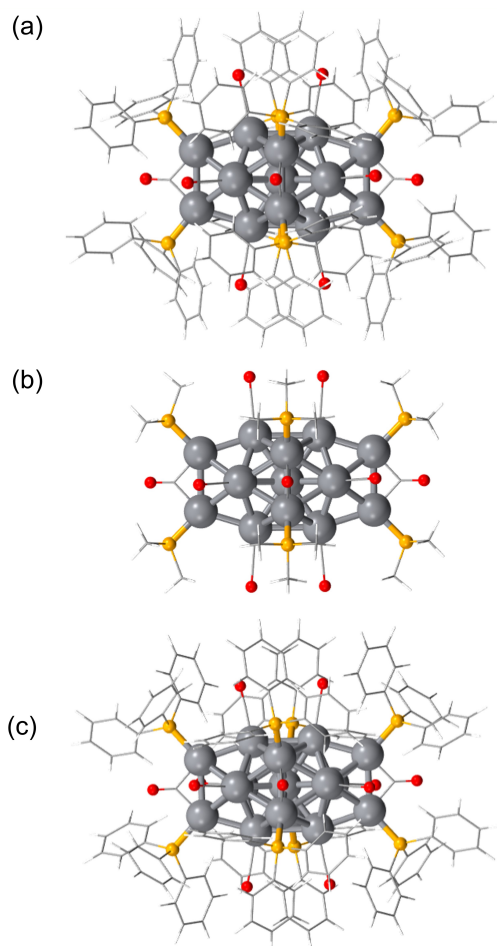
Fig. 2 Geometric structure of (a) $[Pt_{17}(CO)_{12}(PPh_3)_8]^{2+}$ determined by SC-XRD from Ref. 11 and the calculated most stable structures of (b) $Pt_{17}(CO)_{12}(P(CH_3)_3)_8]^{2+}$ and (c) $[Pt_{17}(CO)_{12}(PPh_3)_8]^{2+}$. Hydrogen and solvent atoms are omitted for clarity. Pt: grey, P: yellow, O: red, and carbon: light grey.
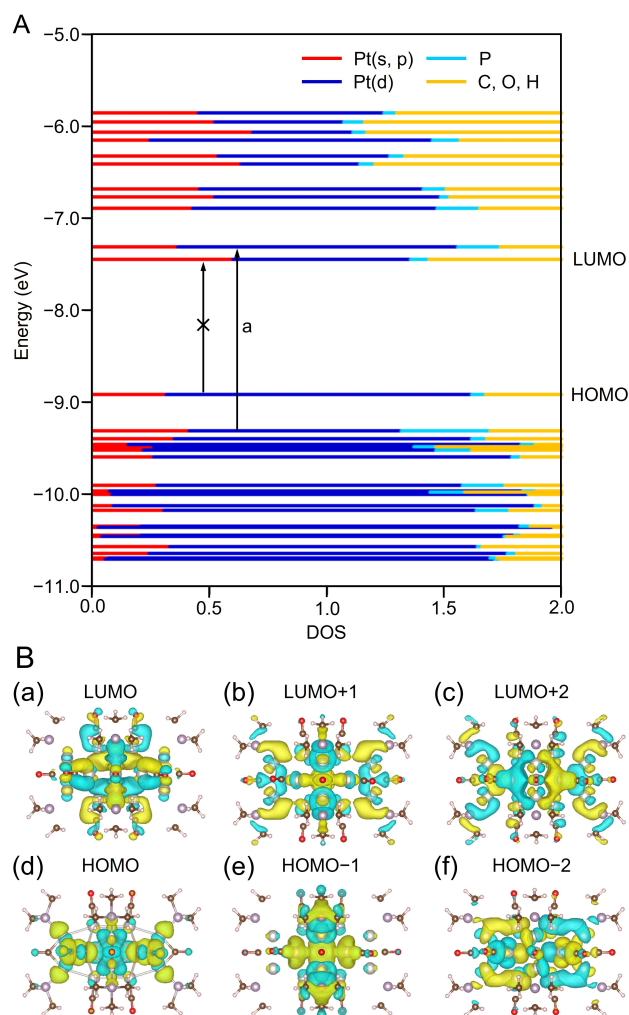
Fig. 4 (A) Calculated energy diagram and (B) related molecular orbitals of $Pt_{17}(CO)_{12}(P(CH_3)_3)_8]^{2+}$. (a) LUMO, (b) LUMO+1, (c) LUMO+2, (d) HOMO, (e) HOMO−1, and (f) HOMO−2 states.

Thus, this study successfully elucidated the electronic structure and the origin of the optical absorption spectrum of $[Pt_{17}(CO)_{12}(PPh_3)_8]^z$ using both experimental and theoretical approaches. These findings align with previous research[43-48] on ligand-protected Au-, Ag-, and Cu NCs. Specifically, several key findings regarding the electronic structure have been observed: 1) a distinct peak structure appears in the optical absorption spectrum when the metal core is refined to ~1 nm;[49-52] 2) the peak structure in the visible region is mainly caused by the absorption of the metal core;[31] 3) differences in the structure of the functional groups at the end of the ligands have negligible effect on optical absorption.[53-55]

Electrocatalytic activity of Pt_{17}/CB for the HER

Having established the geometrical and electronic structures of the Pt NCs, we next aimed to create highly active catalysts by increasing the number of active sites through miniaturization. Although many highly active Pt NCs have been reported,[56-66] most require special equipment and reagents. Accordingly, those methods are not suitable for the preparation of the practical Pt NC catalyst. Although simple methods have also been reported for the preparation of Pt NCs, Pt NCs synthesized by those methods typically includes the variation in the number of constituent atoms. Accordingly, they do not necessarily show high activity specialized in the NC-size region. Therefore, in this work, we attempted to prepare the Pt NC catalysts using $[Pt_{17}(CO)_{12}(PPh_3)_8]^z$, which can be obtained with atomic precision by simple synthesis in air, as a precursor to establish a method for preparing the practical NC catalyst with high HER activity. It can be expected that using such an atomically precise Pt NC as catalyst also help to understand the mechanisms of the HER which occurs over NC catalysts.[66]

In the experiment, following a previously established method with a slight modification,[13] Pt_{17} NCs were supported on CB (Fig. 1c) with a Pt loading of 1.0 wt% through chemisorption, and the ligands were removed by calcination at 200 °C. Transmission electron microscopy (TEM) images of the calcined Pt_{17} NC-supported CB catalyst (Pt_{17}/CB(1.0 wt% Pt)) showed that the particle size of Pt_{17} NC remains largely unchanged during the adsorption and calcination processes (Figs. 5ab and S7). X-ray photoelectron spectroscopy (XPS) indicated that the Pt in Pt_{17}/CB(1.0 wt% Pt) is in a largely metallic electronic state with a slight positive charge, similar to the previously reported one (Figs. 5c and S8).[13]

To evaluate their HER activities, a catalyst slurry was prepared using Pt_{17}/CB(1.0 wt% Pt) and then deposited onto a glassy carbon electrode (GCE) to create the working electrode. After electrochemical cleaning[67] to remove residual organic substances, the HER activity was measured and compared with that of a catalyst made by diluting commercial Pt NPs/CB(46.9 wt% Pt; TEC10E50E) with CB until 1.0 wt% Pt to prepare Pt NPs/CB(1.0 wt% Pt).

Fig. 6a. shows the linear sweep voltammetry (LSV) curves for Pt_{17}/CB(1.0 wt% Pt) and Pt NPs/CB(1.0 wt% Pt). The results show that Pt_{17}/CB(1.0 wt% Pt) generates a larger reduction current than Pt NPs/CB(1.0 wt% Pt) starting around 0.0 V *vs.* reversible hydrogen electrode (RHE), indicating that Pt_{17}/CB(1.0 wt% Pt) has superior HER activity than Pt NPs/CB(1.0 wt% Pt). Comparison of current values at −0.055 V *vs.* RHE with the appropriate Tafel slope in the HER (Fig. 6b) revealed that Pt_{17}/CB(1.0 wt% Pt) has 1.26-times the HER activity (7.54 *vs.*

5.98 mA cm$^{−2}$; Fig. 6c) of Pt NPs/CB(1.0 wt% Pt). Additionally, Pt_{17}/CB(1.0 wt% Pt) provided Tafel slopes similar with theoretical one for the Volmer step of 120 mV/dec assuming that H$^+$ adsorption on the catalyst surface serves as the rate determining step for the two-step HER. The reduction potential at which a current of −10 mA cm$^{−2}$ is obtained, which is commonly used for HER activity comparisons, is −0.075 V *vs.* RHE for Pt_{17}/CB(1.0 wt% Pt), indicating a significantly decreased overvoltage for the HER compared with −0.103 V *vs.* RHE for Pt NPs/CB(1.0 wt% Pt). Furthermore, the obtained mass activity of Pt_{17}/CB(1.0 wt% Pt) at −0.05 V *vs.* RHE is significantly higher than the HER mass activities reported in previous experimental studies using Pt NCs or single-atom Pt catalysts (Table S1).

To evaluate the ease of proton (H$^+$) adsorption, we attempted to calculate the electrochemical surface area (ECSA) based on H$^+$ adsorption from cyclic voltammetry (CV) curves.
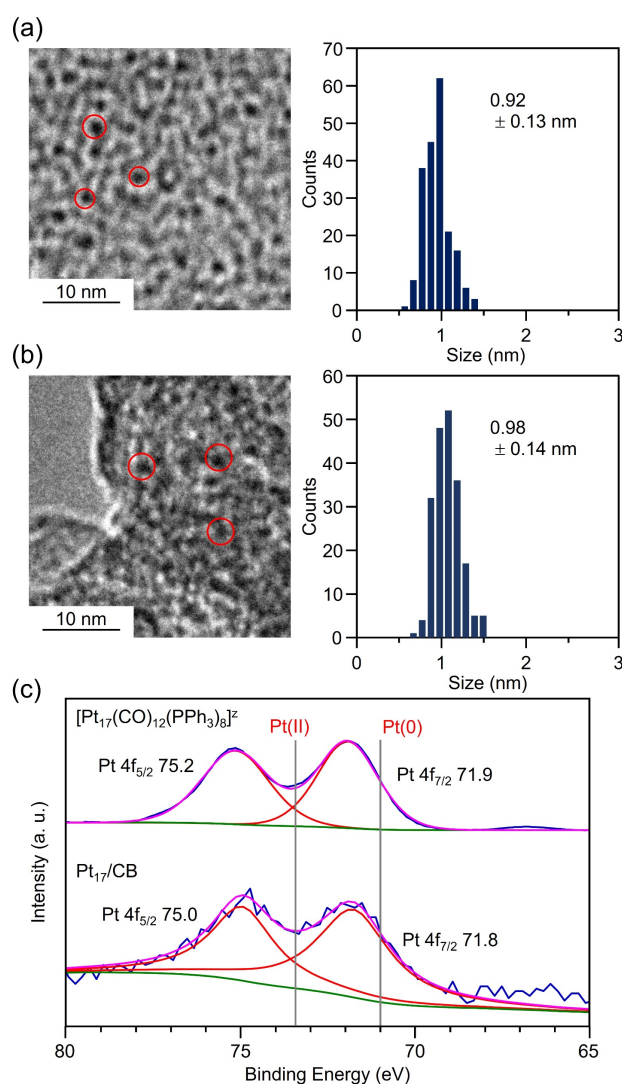
Fig. 5 TEM images and resulting histograms of particle-size distribution for (a) $[Pt_{17}(CO)_{12}(PPh_3)_8]^z$ and (b) Pt_{17}/CB(1.0 wt% Pt). (c) Pt 4f$_{7/2}$ XPS spectra (blue line) and their fitting results (red, green, and magenta lines) for $[Pt_{17}(CO)_{12}(PPh_3)_8]^z$ and Pt_{17}/CB(1.0 wt% Pt). In (c), grey vertical lines indicate the position of Pt(0) and Pt(II).

ARTICLE

Owing to the low Pt loading (1.0 wt% Pt), the current value for H^+ adsorption was insufficient for accurate ECSA calculation. Therefore, we prepared a catalyst with a higher Pt loading (20.0 wt% Pt) for further investigation. Pt_{17}/CB(20.0 wt% Pt) was prepared by loading $[Pt_{17}(CO)_{12}(PPh_3)_8]^z$ at 20.0 wt% Pt followed by calcination using a similar method to that used to prepare Pt_{17}/CB(1.0 wt% Pt). The calcination conditions were more severe (250 °C, 120 min) than for Pt_{17}/CB(1.0 wt% Pt), considering that the number of ligands present on the support also increased. For the obtained Pt_{17}/CB(20.0 wt% Pt), a slight increase in average particle size based on the aggregation of Pt_{17} NCs was observed (Fig. S9). This is thought to be because Pt_{17}

NCs were mainly loaded on CB by physisorption, different from the case of Pt_{17}/CB(1.0 wt% Pt). Because of such a weak interaction between Pt_{17} NCs and CB, a part of Pt_{17} NCs aggregated during the calcination process. Electrochemical cleaning was performed on the obtained Pt_{17}/CB(20.0 wt% Pt), followed by electrochemical measurements. A commercial catalyst (TEC10E50E; Pt NPs/CB(46.9 wt% Pt)) was used as a comparison (Fig. S10). HER mass activity at different Pt loadings was also calculated and compared. As a result, Pt_{17}/CB(20.0 wt% Pt) showed 3.59-times the HER mass activity (1.76 *vs.* 0.49 A mg$^{-1}_{Pt}$ at −0.055 V *vs.* RHE; Fig. S11 and Fig. 7) than Pt NPs/CB(46.9 wt% Pt).

In terms of the ECSAs estimated by H^+ adsorption, Pt_{17}/CB(20.0 wt% Pt) has 1.07-times (101.3 *vs.* 94.6 m² g$^{-1}_{Pt}$; Fig. S12a) that of Pt NPs/CB(46.9 wt% Pt). Thus, the activity enhancement of Pt_{17}/CB(20.0 wt% Pt) compared with Pt NPs/CB(46.9 wt% Pt) is higher than that of ECSA. Consequently, when specific activity (SA), the activity per surface active site, is calculated by dividing ECSA by HER mass activity, Pt_{17}/CB(20.0 wt% Pt) shows 3.39-times the SA than that of Pt NPs/CB(46.9 wt% Pt) (Fig. S12b). Although it is difficult to accurately calculate the active site by ECSA because, unlike Pt NPs, no specific crystalline planes are exposed in Pt_{17}NCs, our estimation implies that the Pt atoms of Pt_{17} NCs might have better HER properties than those of Pt NPs. Therefore, it is reasonable to expect that further improvement in activity can be achieved if it becomes possible to prepare catalysts with a higher Pt loading ratio while suppressing the aggregation of Pt_{17}NCs.

Mechanism of HER activity for Pt_{17}/CB

We examined the origins of the high HER activity of Pt_{17}/CB. Recent studies have suggested that miniaturization creates surface Pt atoms with diverse electronic states, and that high activity occurs when these electronic states are favourable for the progression of reactions.[68,69] In our previous study,[13] DFT calculations revealed that in the optimized structure of Pt_{17}/graphite (Fig. 8A), Pt atoms with various charges and local DOSs are mixed (Fig. S13). Specifically, it was revealed that 1) two Pt atoms (*I* = 6 and 12) contact the graphite, 2) Pt atoms on terraces (*I* = 1, 4, 7, and 17) are positively charged, and 3) Pt atoms at steps and corners (*I* = 2, 3, 5, 8–11, and 13–16) are
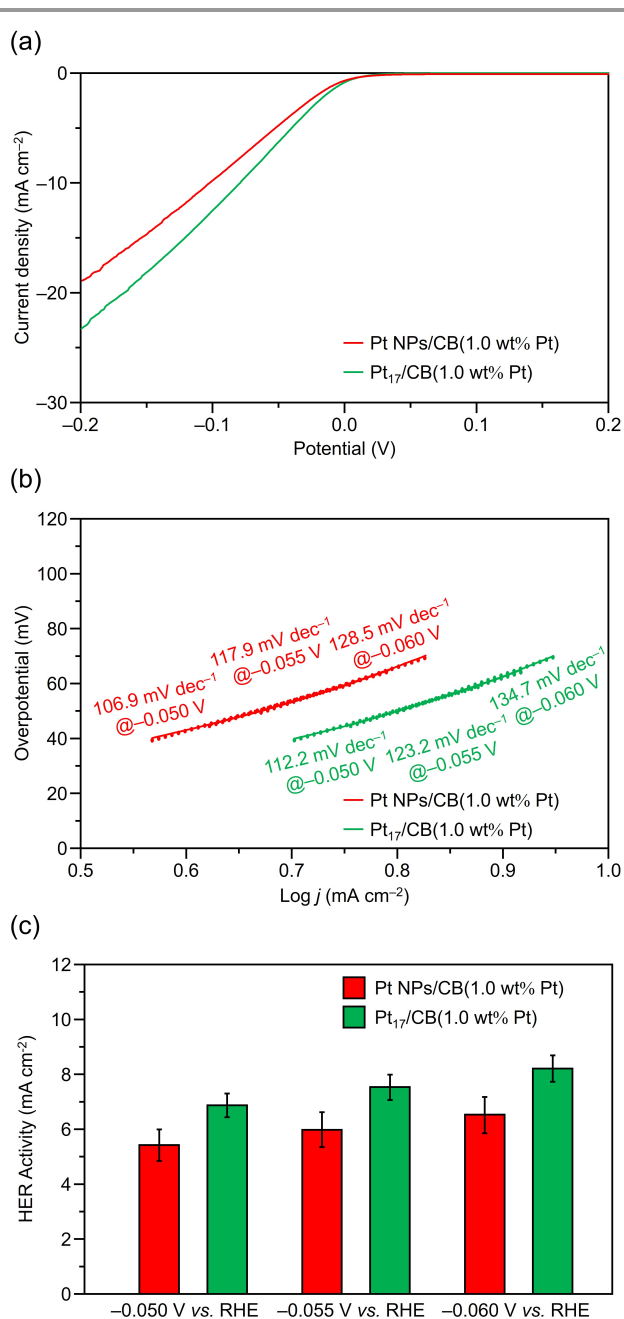
Fig. 6 (a) Representative LSV curves. (b) Tafel slopes and (c) HER activity of Pt_{17}/CB(1.0 wt% Pt) and Pt NPs/CB(1.0 wt% Pt). For (b) and (c), data obtained at −0.050, −0.055, and −0.060 V *vs.* RHE are also shown for comparison.
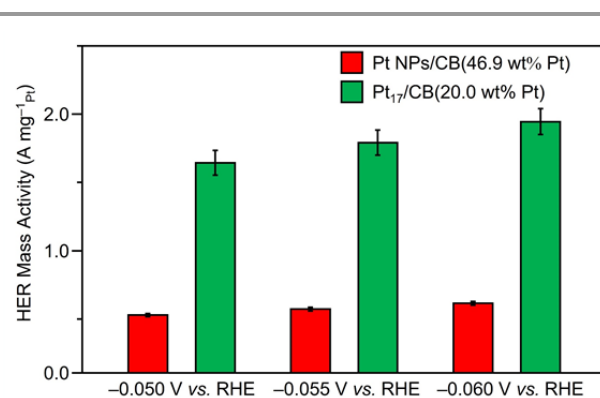
Fig. 7 HER mass activity of Pt_{17}/CB(20.0 wt% Pt) and Pt NPs/CB(46.9 wt% Pt) obtained from the LSVs in Fig. S11. Data obtained at −0.050, −0.055, and −0.060 V *vs.* RHE are also shown for comparison.
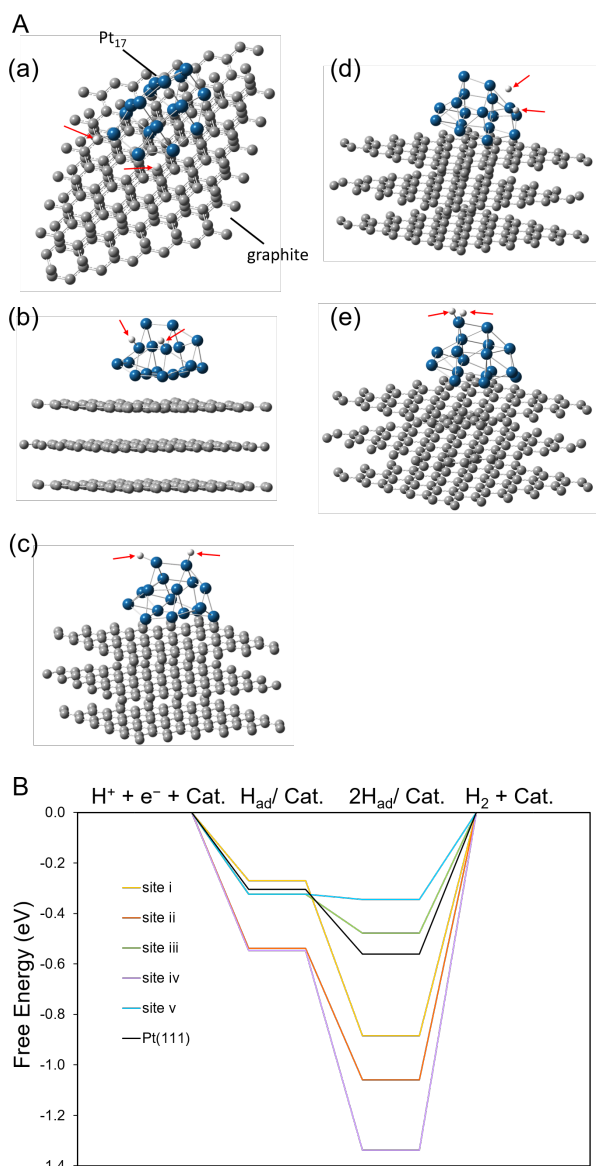
negatively charged. These calculations used graphite as a support instead of CB to reduce computational costs and employed the TEM-observed structure of $Pt_{17}NCs$ as the initial configuration, which was then optimized.[13]

To obtain insights into the HER mechanisms on Pt_{17}/graphite, we optimized the structures of reaction intermediates for the HER. In the calculation, four pairs of Pt atoms (Fig. S13) were selected as potential adsorption sites for hydrogen atoms (H_{ads}) on the Pt_{17}/graphite surface, referred to as $Pt_{17}(X)$/graphite (X = i, ii, iii, or iv). The reaction intermediates (H_{ads}/$Pt_{17}(X)$/graphite) were then obtained by adsorbing H_{ads} onto $Pt_{17}(X)$/graphite (X = i, ii, iii, or iv). In the calculation of the intermediates, we also found another structure

Fig. 8 Results of DFT calculations. (A) Intermediate structure optimized for (a) (H + H)/Pt_{17}(i)/graphite, (b) (H + H)/Pt_{17}(ii)/graphite, (c) (H + H)/Pt_{17}(iii)/graphite (d) (H + H)/Pt_{17}(iv)/graphite and (e) (H + H)/Pt_{17}(v)/graphite. (B) Free-energy diagram for Volmer-Tafel mechanism in HER on $Pt_{17}(X)$/graphite (X = i, ii, iii or iv) or Pt(111) under an applied potential of 0.0 V *vs.* SHE. In this figure, $Pt_{17}(X)$/graphite and Pt(111) are abbreviated as Cat. In (A), the red arrows indicate adsorbed H.

in which the pair of H_{ads} is on the identical Pt atom (l = 11), referred to as Pt_{17}(v)/graphite.

The HER generally proceeds through two main pathways. Initially, H^+ is adsorbed and reduced as H_{ads} on the electrode surface (the Volmer step). Subsequently, the reaction can proceed through either: 1) the combination of two H_{ads} to form H_2, which then desorbs (the Volmer–Tafel mechanism), or 2) the incorporation of another H^+ and electron onto H_{ads} to form H_2, which then desorbs (the Volmer–Heyrovsky mechanism). Here, the mechanism by which the reaction proceeds depends largely on the electrode material. In the case of the Pt(111) surface, which is considered to be present in Pt NPs/CB, the HER is likely to proceed by the Volmer–Tafel mechanism with Tafel step being the rate-limiting step.[70,71] Thus, we have calculated the reaction when it proceeds by the Volmer–Tafel mechanism (Fig. 8B). The free-energy change in the Tafel process in Pt_{17}(iii)/graphite and Pt_{17}(v)/graphite was smaller than that of Pt(111). From the slope of the current-potential curve obtained in the experiment (Fig. 6b), the rate-limiting step of Pt_{17}/CB was found to be Volmer step, different from the case of Pt(111). Probably, there are reaction pathways with a low Tafel barrier (such as site iii and v) in Pt_{17}/graphite, and these reaction sites are presumed to have changed the rate-limiting step to Volmer step.[72,73] This HER energy diagram implies that the smaller H adsorption energy on $Pt_{17}(X)$/graphite comparted to that on a large Pt nanoparticle causes the high HER activity of Pt_{17}/CB(20.0 wt% Pt), although it is difficult to demonstrate this computationally. Note that the rate-limiting step of Pt NPs/CB was also Volmer step in our experiment (Fig. 6b). It is presumed that in the Pt NPs/CB, small and highly active NCs also exist and they mainly contribute to the activity of Pt NPs/CB shown in Figure 6(a).

Finally, we discuss about the reason why H adsorption energy on $Pt_{17}(X)$/graphite is smaller than that on a large Pt NP. The variation in the H adsorption energy is attributed to three factors. The first factor is the H adsorption structure. The bridge positions in sites i and iv results in the large stabilization of H_{ads} than the ontop positions. The second is the low coordination-number site in $Pt_{17}(X)$/graphite. The pair of H_{ads} on the identical Pt atom (l = 11) at the site v results in the small adsorption energy. The last is variety in the electronic property among the Pt atoms of $Pt_{17}(X)$/graphite. In the case of site iii (l = 9, 11), both H_{ads} are bounded to Pt in the ontop manner. In addition, in this structure, both Pt atoms are negatively charged (Table S13). Accordingly, both H_{ads} on site iii are negatively charged (Table S2). Although the higher electronegativity of Pt compared with H (2.28 for Pt *cf.* 2.20 for H, respectively) could promote the electron transfer from H to Pt, a negatively charged Pt atom is less likely to facilitate electron transfer from H to Pt, causing the less stabilization. Accordingly, the adsorption of H_{ads} is weak at site iii, and thereby HER progression occurs easier than at other reaction sites. This is in contrast to site ii where both H_{ads} are on the ontop position in a similar manner to the case of site iii. In this case, the pair of Pt atoms at site ii are positively charged, resulting in the strong adsorption of H via the electron transfer from H to Pt.

Conclusion

In this study, we used DFT calculations to elucidate the origin of the electronic structure of $[Pt_{17}(CO)_{12}(PPh_3)_8]^z$ with atomic precision.

Furthermore, the HER activity of Pt_{17}/CB catalysts using $[Pt_{17}(CO)_{12}(PPh_3)_8]^z$ as a precursor was evaluated. The origin of the high HER activity of the Pt_{17}/CB catalyst was also investigated using DFT calculations. As a result, the following conclusions were obtained:

1) The HOMO-to-LUMO transition in $[Pt_{17}(CO)_{12}(PPh_3)_8]^{2+}$ is forbidden, with nearby orbitals primarily comprising the s, p, and d orbitals of Pt.

2) Pt_{17}/CB(20.0 wt% Pt) exhibits 3.59-times the HER mass activity of the commercial Pt NPs/CB(46.9 wt% Pt) catalyst.

3) Pt_{17}/graphite generates surface Pt atoms more favourable for the HER than the Pt(111) surface in Pt NPs/CB, leading to higher HER activity.

These findings offer clear design guidelines for understanding the electronic structure of atomically precise Pt NCs, developing highly active HER catalysts using Pt NCs, and reducing Pt usage in PEMWE applications. It is also expected that alloying these NCs will lead to the creation of even more active catalysts.

Author contribution

Conflicts of interest

The authors declare there are no conflicts of interest.

Data availability

Relevant data are available from the corresponding authors (T. Kawawaki, K. Iida and Y. Negishi) upon reasonable request.

Acknowledgments

References

1 I. Ciabatti, C. Femoni, M. C. Iapalucci, G. Longoni and S. Zacchini, *J. Cluster Sci.*, 2014, **25**, 115–146.

2 M. Paolieri, I. Ciabatti and M. Fontani, *J. Cluster Sci.*, 2019, **30**, 1623–1631.

3 S. S. Kurasov, N. K. Eremenko, Y. L. Slovokhotov and Y. T. Struchkov, *J. Organomet. Chem.*, 1989, **361**, 405–408.

4 N. d. Silva and L. F. Dahl, *Inorg. Chem.*, 2005, **44**, 9604–9606.

5 I. Ciabatti, C. Femoni, M. C. Iapalucci, G. Longoni, T. Lovato and S. Zacchini, *Inorg. Chem.*, 2013, **52**, 4384–4395.

6 B. Berti, C. Femoni, M. C. Iapalucci, S. Ruggieri and S. Zacchini, *Eur. J. Inorg. Chem.*, 2018, **2018**, 3285–3296.

7 T. Kawawaki, N. Shimizu, K. Funai, Y. Mitomi, S. Hossain, S. Kikkawa, D. J. Osborn, S. Yamazoe, G. F. Metha and Y. Negishi, *Nanoscale*, 2021, **13**, 14679–14687.

8 T. Kawawaki, N. Shimizu, Y. Mitomi, D. Yazaki, S. Hossain and Y. Negishi, *Bull. Chem. Soc. Jpn.*, 2021, **94**, 2853–2870.

9 D. Yazaki, T. Kawawaki, D. Hirayama, M. Kawachi, K. Kato, S. Oguchi, Y. Yamaguchi, S. Kikkawa, Y. Ueki, S. Hossain, D. J. Osborn, F. Ozaki, S. Tanaka, J. Yoshinobu, G. F. Metha, S. Yamazoe, A. Kudo, A. Yamakata and Y. Negishi, *Small*, 2023, **19**, 2208287.

10 D. Yazaki, T. Kawawaki, T. Tanaka, D. Hirayama, Y. Shingyouchi and Y. Negishi, *Energy Adv.*, 2023, **2**, 1148–1154.

11 L. V. Nair, S. Hossain, S. Wakayama, S. Takagi, M. Yoshioka, J. Maekawa, A. Harasawa, B. Kumar, Y. Niihori, W. Kurashige and Y. Negishi, *J. Phys. Chem. C*, 2017, **121**, 11002–11009.

12 C. Schmitt, N. D. Roit, M. Neumaier, C. B. Maliakkal, D. Wang, T. Henrich, C. Kübel, M. Kappes and S. Behrens, *Nanoscale Adv.*, 2024, **6**, 2459–2468.

13 T. Kawawaki, Y. Mitomi, N. Nishi, R. Kurosaki, K. Oiwa, T. Tanaka, H. Hirase, S. Miyajima, Y. Niihori, D. J. Osborn, T. Koitaya, G. F. Metha, T. Yokoyama, K. Iida and Y. Negishi, *Nanoscale*, 2023, **15**, 7272–7279.

14 S. Reid and H. Hernández, *J. Phys. Chem. A*, 2023, **127**, 4237–4244.

15 A. K. Satheesan, L. V. Nair, J. S. Gopinath, P. Parameswaran and C. Keloth, *J. Phys. Chem. C*, 2023, **127**, 568–576.

16 J. Wei, R. Marchal, D. Astruc, S. Kahlal, J.-F. Halet and J.-Y. Saillard, *Nanoscale*, 2022, **14**, 3946–3957.

17 A. K. Satheesan, N. P. Purayil, J. Singh and C. Keloth, *ACS Appl. Nano Mater.*, 2024, **7**, 7486–7495.

18 J. M. Guevara-Vela, T. Rocha-Rinza, P. L. Rodríguez-Kessler and A. Muñoz-Castro, *Phys. Chem. Chem. Phys.*, 2023, **25**, 28835–28840.

19 H. Hirase, K. Iida and J.-y. Hasegawa, *Phys. Chem. Chem. Phys.*, 2024, DOI: 10.1039/D4CP00555D.

20 J. Zhu, L. Hu, P. Zhao, L. Y. S. Lee and K.-Y. Wong, *Chem. Rev.*, 2020, **120**, 851–918.

21 M. Chatenet, B. G. Pollet, D. R. Dekel, F. Dionigi, J. Deseure, P. Millet, R. D. Braatz, M. Z. Bazant, M. Eikerling, I. Staffell, P. Balcombe, Y. Shao-Horn and H. Schäfer, *Chem. Soc. Rev.*, 2022, **51**, 4583–4762.

22 J. N. Hansen, H. Prats, K. K. Toudahl, N. M. Secher, K. Chan, J. Kibsgaard and I. Chorkendorff, *ACS Energy Lett.*, 2021, **6**, 1175–1180.

23 C. C. L. McCrory, S. Jung, I. M. Ferrer, S. M. Chatman, J. C. Peters and T. F. Jaramillo, *J. Am. Chem. Soc.*, 2015, **137**, 4347–4357.

24 F. Fievet, J. P. Lagier and M. Figlarz, *MRS Bull.*, 2013, **14**, 29–34.

25 C. Bock, C. Paquet, M. Couillard, G. A. Botton and B. R. MacDougall, *J. Am. Chem. Soc.*, 2004, **126**, 8028–8037.

26 H. Dong, Y.-C. Chen and C. Feldmann, *Green Chem.*, 2015, **17**, 4107–4132.

27 C. M. Pelicano, M. Saruyama, R. Takahata, R. Sato, Y. Kitahama, H. Matsuzaki, T. Yamada, T. Hisatomi, K. Domen and T. Teranishi, *Adv. Funct. Mater.*, 2022, **32**, 2202987.

28 B.-J. Hwang, L. S. Sarma, C.-H. Chen, C. Bock, F.-J. Lai, S.-H. Chang, S.-C. Yen, D.-G. Liu, H.-S. Sheu and J.-F. Lee, *J. Phys. Chem. C*, 2008, **112**, 19922–19929.

29 I. Schrader, J. Warneke, S. Neumann, S. Grotheer, A. A. Swane, J. J. K. Kirkensgaard, M. Arenz and S. Kunz, *J. Phys. Chem. C*, 2015, **119**, 17655–17661.

30 Y. Negishi, N. Shimizu, K. Funai, R. Kaneko, K. Wakamatsu, A. Harasawa, S. Hossain, M. E. Schuster, D. Ozkaya, W. Kurashige, T. Kawawaki, S. Yamazoe and S. Nagaoka, *Nanoscale Adv.*, 2020, **2**, 669–678.

31 M. Zhu, C. M. Aikens, F. J. Hollander, G. C. Schatz and R. Jin, *J. Am. Chem. Soc.*, 2008, **130**, 5883–5885.

32 M. W. Heaven, A. Dass, P. S. White, K. M. Holt and R. W. Murray, *J. Am. Chem. Soc.*, 2008, **130**, 3754–3755.

33 C. M. Aikens, *J. Phys. Chem. A*, 2009, **113**, 10811–10817.

34 M. J. Hartmann, H. Häkkinen, J. E. Millstone and D. S. Lambrecht, *J. Phys. Chem. C*, 2015, **119**, 8290–8298.

35 M. J. Frisch, G. W. Trucks, H. B. Schlegel, G. E. Scuseria, M. A. Robb, J. R. Cheeseman, G. Scalmani, V. Barone, G. A. Petersson, H. Nakatsuji, X. Li, M. Caricato, A. V. Marenich, J. Bloino, B. G. Janesko, R. Gomperts, B. Mennucci, H. P. Hratchian, J. V. Ortiz, A. F. Izmaylov, J. L. Sonnenberg, D. Williams-Young, F. Ding, F. Lipparini, F. Egidi, J. Goings, B. Peng, A. Petrone, T. Henderson, D. Ranasinghe, V. G. Zakrzewski, J. Gao, N. Rega, G. Zheng, W. Liang, M. Hada, M. Ehara, K. Toyota, R. Fukuda, J. Hasegawa, M. Ishida, T. Nakajima, Y. Honda, O. Kitao, H. Nakai, T. Vreven, K. Throssell, J. A. Montgomery, Jr., J. E. Peralta, F. Ogliaro, M. J. Bearpark, J. J. Heyd, E. N. Brothers, K. N. Kudin, V. N. Staroverov, T. A. Keith, R. Kobayashi, J. Normand, K. Raghavachari, A. P. Rendell, J. C. Burant, S. S. Iyengar, J. Tomasi, M. Cossi, J. M. Millam, M. Klene, C. Adamo, R. Cammi, J. W. Ochterski, R. L. Martin, K. Morokuma, O. Farkas, J. B. Foresman and D. J. Fox, *Gaussian 16, Revision C.01*, Gaussian, Inc., Wallingford CT, 2016.

36 A. D. Becke, *Phys. Rev. A*, 1988, **38**, 3098–3100.

37 C. Lee, W. Yang and R. G. Parr, *Phys. Rev. B*, 1988, **37**, 785–789.

38 A. D. Becke, *J. Chem. Phys.*, 1993, **98**, 5648–5652.

39 M. Dolg, U. Wedig, H. Stoll and H. Preuss, *J. Chem. Phys.,* 1987, **86**, 866–872.

40 K. A. Kacprzak, L. Lehtovaara, J. Akola, O. Lopez-Acevedo and H. Häkkinen, *Phys. Chem. Chem. Phys.*, 2009, **11**, 7123–7129.

41 P. J. Hay and W. R. J. Wadt, *J. Chem. Phys.*, 1985, **82**, 299–310.

42 T. H. Dunning Jr. and P. J. Hay, in Modern Theoretical Chemistry, Ed. H. F. Schaefer III, Plenum, New York, 1976, **3**, 1–28.

43 B. Yin and Z. Luo, *Coord. Chem. Rev.*, 2021, **429**, 213643.

44 T. Kawawaki, Y. Imai, D. Suzuki, S. Kato, I. Kobayashi, T. Suzuki, R. Kaneko, S. Hossain and Y. Negishi, *Chem. - Eur. J.*, 2020, **26**, 16150–16193.

45 X. Kang, Y. Li, M. Zhu and R. Jin, *Chem. Soc. Rev.*, 2020, **49**, 6443–6514.

46 J. Fang, B. Zhang, Q. Yao, Y. Yang, J. Xie and N. Yan, *Coord. Chem. Rev.*, 2016, **322**, 1–29.

47 I. Chakraborty and T. Pradeep, *Chem. Rev.*, 2017, **117**, 8208–8271.

48 Y. Du, H. Sheng, D. Astruc and M. Zhu, *Chem. Rev.*, 2020, **120**, 526–622.

49 T. Kawawaki and Y. Negishi, *Dalton Trans.*, 2023, **52**, 15152–15167.

50 K. Kwak, V. D. Thanthirige, K. Pyo, D. Lee and G. Ramakrishna, *J. Phys. Chem. Lett.*, 2017, **8**, 4898–4905.

51 M. Zhou, C. Zeng, Y. Song, J. W. Padelford, G. Wang, M. Y. Sfeir, T. Higaki and R. Jin, *Angew. Chem. Int. Ed.*, 2017, **56**, 16257–16261.

52 M. Zhou, X. Du, H. Wang and R. Jin, *ACS Nano*, 2021, **15**, 13980–13992.

53 Y. Song, J. Zhong, S. Yang, S. Wang, T. Cao, J. Zhang, P. Li, D. Hu, Y. Pei and M. Zhu, *Nanoscale*, 2014, **6**, 13977–13985.

54 S. Takano, S. Ito and T. Tsukuda, *J. Am. Chem. Soc.*, 2019, **141**, 15994–16002.

55 T. Omoda, S. Takano and T. Tsukuda, *Small*, 2021, **17**, 2001439.

56 W. Liu, Z. Xiang, A. Tan, K. Wan, Z. Fu and Z. Liang, *Adv. Funct. Mater.*, 2023, **33**, 2212752.

57 J. Klein, A. K. Engstfeld, S. Brimaud and R. J. Behm, *Phys. Chem. Chem. Phys.*, 2020, **22**, 19059–19068.

58 J. Han, C. Gong, C. He, P. He, J. Zhang and Z. Zhang, *J. Mater. Chem. A*, 2022, **10**, 16403–16408.

59 Y. Lai, Z. Zhang, Z. Zhang, Y. Tan, L. Yu, W. Wu, Z. Wang, T. Jiang, S. Gao and N. Cheng, *Chem. Eng. J.*, 2022, **435**, 135102.

60 N. Cheng, S. Stambula, D. Wang, M. N. Banis, J. Liu, A. Riese, B. Xiao, R. Li, T.-K. Sham, L.-M. Liu, G. A. Botton and X. Sun, *Nat. Commun.*, 2016, **7**, 13638.

61 Y. Zhao, P. V. Kumar, X. Tan, X. Lu, X. Zhu, J. Jiang, J. Pan, S. Xi, H. Y. Yang, Z. Ma, T. Wan, D. Chu, W. Jiang, S. C. Smith, R. Amal, Z. Han and X. Lu, *Nat. Commun.*, 2022, **13**, 2430.

62 S. Kumari, T. Masubuchi, H. S. White, A. Alexandrova, S. L. Anderson and P. Sautet, *J. Am. Chem. Soc.*, 2023, **145**, 5834–5845.

63 M. Zhou, S. Bao and A. J. Bard, *J. Am. Chem. Soc.*, 2019, **141**, 7327–7332.

64 Z. Zeng, S. Küspert, S. E. Balaghi, H. E. M. Hussein, N. Ortlieb, M. Knäbbeler-Buß, P. Hügenell, S. Pollitt, N. Hug, J. Melke and A. Fischer, *Small*, 2023, **19**, 2205885.

65 C. Dong, Y. Li, D. Cheng, M. Zhang, J. Liu, Y.-G. Wang, D. Xiao and D. Ma, *ACS Catal.*, 2020, **10**, 11011–11045.

66 R. Wang, D. Chen, L. Fang, W. Fan, Q. You, G. Bian, Y. Zhou, W. Gu, C. Wang, L. Bai, J. Li, H. Deng, L. Liao, J. Yang and Z. Wu, *Angew. Chem. Int. Ed.*, 2024, **63**, e202402565.

67 Y. Lu, Y. Jiang, X. Gao and W. Chen, *Chem. Commun.*, 2014, **50**, 8464–8467.

68 F. Calle-Vallejo, J. Tymoczko, V. Colic, Q. H. Vu, M. D. Pohl, K. Morgenstern, D. Loffreda, P. Sautet, W. Schuhmann and A. S. Bandarenka, *Science*, 2015, **350**, 185–189.

69 B. Garlyyev, J. Fichtner, O. Piqué, O. Schneider, A. S. Bandarenka and F. Calle-Vallejo, *Chem Sci*, 2019, **10**, 8060–8075.

70 G. Ramos-Sanchez and P. B. Balbuena, *Phys. Chem. Chem. Phys.*, 2013, **15**, 11950–11959.

71 E. Skúlason, V. Tripkovic, M. E. Björketun, S. Gudmundsdóttir, G. Karlberg, J. Rossmeisl, T. Bligaard, H. Jónsson and J. K. Nørskov, *J. Phys. Chem. C*, 2010, **114**, 18182–18197.

72 S. Kumari, T. Masubuchi, H. S. White, A. Alexandrova, S. L. Anderson and P. Sautet, *J. Am. Chem. Soc.*, 2023, **145**, 5834–5845.

73 M. Zhou, S. Bao and A. J. Bard, *J. Am. Chem. Soc.*, 2019, **141**, 7327–7332.